Supporting information for

Two-dimensional Janus pentagonal MSeTe (M = Ni, Pd, Pt): promising water-splitting photocatalysts and opto-electronic materials

Yu-Xun Yuan[1], Lu Pan[1], Zhao-Qi Wang [2,*], Zhao-Yi Zeng[3], Hua-Yun Geng [4], Xiang-Rong Chen [1,*]

[1] College of Physics, Sichuan University, Chengdu 610064, China;

[2] College of Science, Xian University of Science and Technology, Xian 710054, China;

[3] College of Physics and Electronic Engineering, Chongqing Normal University, Chongqing 400047, China;

[4] National Key Laboratory for Shock Wave and Detonation Physics Research, Institute of Fluid Physics, CAEP, Mianyang 621900, China

ABSTRACT

Inspired by the interesting and novel properties exhibited by Janus transition metal dichalcogenides (TMDs) and two-dimensional pentagonal structures, we here investigated the structural stability, mechanical, electronic photocatalytic, and optical properties for a class of two-dimensional (2D) pentagonal Janus TMDs, namely penta-MSeTe (M = Ni, Pd, Pt) monolayers, by using density functional theory (DFT) combined with Hubbard's correction (U). Our results showed that these monolayers exhibit well structural stability, proper band structures for photocatalysts, high visible light absorption, and good photocatalytic applicability. The calculated electronic properties reveal that the penta-MSeTe are semiconductors with bandgap range of 2.06-2.39 eV, and their band edge positions meet the requirements for water-splitting photocatalysts in various environment (pH = 0-13). We used stress engineering to seek

* *Corresponding authors. E-mail: zhqwangsc@foxmail.com; xrchen@scu.edu.cn*

higher solar-to-hydrogen (STH) efficiency in acidic (pH=0), neutral (pH=7) and alkaline (pH=13) environments for penta-MSeTe through 0% to +8% biaxial and uniaxial strain. Our results showed that penta-PdSeTe stretched 8% along y direction demonstrates STH efficiency as high as 29.71% when pH=0, which break the theoretical limit of conventional photocatalytic model. We also calculated the optical properties and found that they exhibit high absorption (13.11%) in the visible light range and own diverse range of hyperbolic regions. Hence, it is anticipated that penta-MSeTe materials hold great promise for applications in photocatalytic water splitting and optoelectronic devices.

Table S1 Elastic constants ($C_{11}, C_{22}, C_{12}, C_{66}$) and Young's modulus ($Y_x$, Y_y: the Y value along the x, y direction) of the penta-MSeTe (M = Ni, Pd, Pt) monolayers.

Materials	$C_{11}(Nm^{-1})$	$C_{22}(Nm^{-1})$	$C_{12}(Nm^{-1})$	$C_{66}(Nm^{-1})$	$Y_x(Nm^{-1})$	$Y_y(Nm^{-1})$
NiSeTe	24.25	62.88	-3.29	25.35	24.08	62.44
PdSeTe	27.70[8]	53.61	0.073	18.16	27.70	53.61
PtSeTe	35.46	65.57	0.80	23.29	35.45	65.55

Table S2 The band gaps and band edges information of the penta-MSeTe (M = Ni, Pd, Pt) using various methods. Energy is in eV and had been deducted Fermi energy.

Materials	E_{gap}^{PBE}	E_{CBM}^{PBE}	E_{VBM}^{PBE}	$E_{gap}^{PBE+SOC}$	$E_{CBM}^{PBE+SOC}$	E_{VBM}^{PBE+SO}	E_{gap}^{HSE06}	E_{CBM}^{HSE06}	E_{VBM}^{HSE06}	$E_{gap}^{HSE06+SOC}$	$E_{CBM}^{HSE06+SOC}$	$E_{VBM}^{HSE06+SO}$
NiSeTe	0.97	-2.17	-3.14	0.90	-2.18	-3.08	2.05	-1.94	-3.99	1.98	-1.96	-3.94
NiSeTe+U	1.39	-2.05	-3.44	1.26	-2.12	-3.38	2.39	-1.70	-4.09	2.30	-1.72	-4.02
PdSeTe	1.30	-2.01	-3.31	1.22	-2.03	-3.25	2.04	-1.86	-3.90	1.97	-1.89	-3.86
PdSeTe+U	1.33	-2.01	-3.34	1.27	-2.01	-3.28	2.07	-1.85	-3.92	2.00	-1.88	-3.88
PtSeTe	1.42	-1.89	-3.31	1.21	-2.04	-3.25	2.03	-1.88	-3.91	2.13	-1.69	-3.82
PtSeTe+U	1.49	-1.86	-3.35	1.34	-1.71	-3.05	2.30	-1.64	-3.94	2.22	-1.65	-3.87

Table S3 The band gap (E_{gap}), the difference of the electrostatic potential ($\Delta\Phi$), CBM (E_{CBM}) and VBM (E_{VBM}) refer to the vacuum level, over-potential for hydrogen evolution reaction $\chi(H_2)$, the over-Potential for oxygen evolution reaction $\chi(O_2)$, energy conversion efficiency of light absorption (η_{abs}), carrier utilization (η_{cu}) and STH (η_{STH}) efficiency in acidic (pH = 0) environment.

Materials		E_{gap} (eV)	$\Delta\Phi$ (eV)	E_{CBM} (eV)	E_{VBM} (eV)	$\chi(H_2)$ (eV)	$\chi(O_2)$ (eV)	η_{abs} (%)	η_{cu} (%)	η_{STH} (%)
Biaxial Strain	NiSeTe (0%)	2.386	0.373	-3.829	-6.215	0.984	0.545	21.59	39.60	8.55
	NiSeTe (2%)	2.322	0.344	-3.916	-6.238	0.868	0.568	23.74	42.23	10.03
	NiSeTe (4%)	2.126	0.317	-4.141	-6.267	0.616	0.597	31.17	46.90	14.62
	NiSeTe (6%)	1.961	0.291	-4.341	-6.302	0.390	0.632	38.29	49.61	18.99
	NiSeTe (8%)	1.817	0.266	-4.511	-6.328	0.195	0.658	45.31	51.81	23.47
	PdSeTe (0%)	2.068	0.409	-4.024	-6.092	0.825	0.422	33.66	35.90	12.08
	PdSeTe (2%)	1.815	0.384	-4.300	-6.115	0.524	0.445	45.44	41.22	18.73
	PdSeTe (4%)	1.538	0.361	-4.607	-6.145	0.194	0.475	59.54	48.37	28.80
	PtSeTe (0%)	2.297	0.422-	-3.882	-6.179	0.980	0.509	24.67	38.08	9.40
	PtSeTe (2%)	2.212	0.401	-4.006	-6.218	0.835	0.548	27.88	42.14	11.75
	PtSeTe (4%)	2.093	0.382	-4.172	-6.264	0.650	0.594	32.49	47.37	15.39
	PtSeTe (6%)	1.851	0.365	-4.466	-6.317	0.339	0.647	43.62	51.01	22.25
X Strain	NiSeTe (2%)	2.383	0.346	-3.862	-6.245	0.924	0.575	21.59	42.15	9.10
	NiSeTe (4%)	2.339	0.329	-3.931	-6.270	0.838	0.600	23.12	44.40	10.27
	NiSeTe (6%)	2.243	0.313	-4.050	-6.293	0.703	0.623	26.66	45.64	12.17
	NiSeTe (8%)	2.144	0.297	-4.165	-6.309	0.572	0.639	30.42	46.93	14.27
	PdSeTe (2%)	1.965	0.433	-4.156	-6.121	0.717	0.451	38.14	39.49	15.06
	PdSeTe (4%)	1.827	0.419	-4.308	-6.135	0.551	0.465	44.89	42.31	18.99
	PdSeTe (6%)	1.690	0.406	-4.463	-6.153	0.383	0.483	51.62	46.38	23.94
	PdSeTe (8%)	1.553	0.394	-4.617	-6.169	0.217	0.499	58.57	50.18	29.44
	PtSeTe (2%)	2.276	0.445	-3.928	-6.204	0.957	0.534	25.43	40.05	10.18
	PtSeTe (4%)	2.246	0.432	-3.975	-6.221	0.897	0.551	26.51	41.83	11.09
	PtSeTe (6%)	2.207	0.419	-4.031	-6.237	0.828	0.567	28.03	43.71	12.25

	PtSeTe (8%)	2.155	0.407	-4.098	-6.252	0.749	0.582	29.97	45.64	13.68
Y Strain	NiSeTe (2%)	2.335	0.346	-3.887	-6.222	0.899	0.552	23.28	40.68	9.47
	NiSeTe (4%)	2.244	0.329	-3.972	-6.216	0.797	0.546	26.66	41.59	11.09
	NiSeTe (6%)	2.151	0.315	-4.059	-6.211	0.700	0.541	30.12	42.62	12.83
	NiSeTe (8%)	2.045	0.303	-4.149	-6.194	0.594	0.524	34.54	43.10	14.89
	PdSeTe (2%)	1.948	0.435	-4.160	-6.108	0.715	0.438	38.99	38.85	15.15
	PdSeTe (4%)	1.795	0.423	-4.315	-6.110	0.548	0.440	46.42	41.30	19.17
	PdSeTe (6%)	1.642	0.414	-4.470	-6.112	0.384	0.442	54.19	44.59	24.17
	PdSeTe (8%)	1.489	0.407	-4.624	-6.113	0.223	0.443	62.08	47.87	29.71
	PtSeTe (2%)	2.235	0.450	-3.974	-6.209	0.916	0.539	26.97	41.11	11.09
	PtSeTe (4%)	2.139	0.443	-4.090	-6.229	0.793	0.559	30.71	44.00	13.51
	PtSeTe (6%)	2.022	0.438	-4.227	-6.250	0.651	0.580	35.57	47.18	16.78
	PtSeTe (8%)	1.896	0.437	-4.375	-6.271	0.502	0.601	41.42	50.68	20.99

Table S4 The band gap (E_{gap}), the difference of the electrostatic potential ($\Delta\Phi$), CBM (E_{CBM}) and VBM (E_{VBM}) refer to the vacuum level, over-potential for hydrogen evolution reaction $\chi(H_2)$, the over-Potential for oxygen evolution reaction $\chi(O_2)$, energy conversion efficiency of light absorption (η_{abs}), carrier utilization (η_{cu}) and STH (η_{STH}) efficiency in neutral (pH = 7) environment.

Materials		E_{gap} (eV)	$\Delta\Phi$ (eV)	E_{CBM} (eV)	E_{VBM} (eV)	$\chi(H_2)$ (eV)	$\chi(O_2)$ (eV)	η_{abs} (%)	η_{cu} (%)	η_{STH} (%)
Biaxial Strain	NiSeTe (0%)	2.386	0.373	-3.829	-6.215	0.571	0.958	21.59	43.86	9.47
	NiSeTe (2%)	2.322	0.344	-3.916	-6.238	0.455	0.981	23.74	44.62	10.59
	NiSeTe (4%)	2.126	0.317	-4.141	-6.267	0.203	1.010	31.17	47.18	14.71
	PdSeTe (0%)	2.068	0.409	-4.024	-6.092	0.412	0.835	33.66	48.03	16.17
	PdSeTe (2%)	1.815	0.384	-4.300	-6.115	0.111	0.858	45.44	45.59	20.72
	PtSeTe (0%)	2.297	0.422	-3.882	-6.179	0.567	0.922	24.67	44.95	11.09
	PtSeTe (2%)	2.212	0.401	-4.006	-6.218	0.422	0.961	27.88	46.06	12.84
	PtSeTe (4%)	2.093	0.382	-4.172	-6.264	0.237	1.007	32.49	47.64	15.48
X Strain	NiSeTe (2%)	2.383	0.346	-3.862	-6.245	0.511	0.988	21.59	43.86	9.47
	NiSeTe (4%)	2.339	0.329	-3.931	-6.270	0.425	1.013	23.12	44.40	10.26
	NiSeTe (6%)	2.243	0.313	-4.050	-6.293	0.290	1.036	26.66	45.64	12.17
	NiSeTe (8%)	2.144	0.297	-4.165	-6.309	0.159	1.052	30.42	42.87	13.34
	PdSeTe (2%)	1.965	0.433	-4.156	-6.121	0.304	0.864	38.14	49.56	18.91
	PdSeTe (4%)	1.827	0.419	-4.308	-6.135	0.138	0.878	44.89	47.33	21.24
	PtSeTe (2%)	2.276	0.445	-3.928	-6.204	0.544	0.947	25.43	45.21	11.50
	PtSeTe (4%)	2.246	0.432	-3.975	-6.221	0.484	0.964	26.51	45.58	12.08
	PtSeTe (6%)	2.207	0.419	-4.031	-6.237	0.415	0.980	28.03	46.11	12.92
	PtSeTe (8%)	2.155	0.407	-4.098	-6.252	0.336	0.995	29.97	46.78	14.02
Y Strain	NiSeTe (2%)	2.335	0.346	-3.887	-6.222	0.486	0.965	23.28	44.46	10.35
	NiSeTe (4%)	2.244	0.329	-3.972	-6.216	0.384	0.959	26.66	45.64	12.17
	NiSeTe (6%)	2.151	0.315	-4.059	-6.211	0.283	0.954	30.12	46.83	14.11
	NiSeTe (8%)	2.045	0.303	-4.149	-6.194	0.181	0.937	34.54	47.06	16.25
	PdSeTe (2%)	1.948	0.435	-4.160	-6.108	0.302	0.851	39.00	49.86	19.44

PdSeTe (4%)	1.795	0.423	-4.315	-6.110	0.135	0.853	46.42	47.73	22.16
PtSeTe (2%)	2.235	0.450	-3.974	-6.209	0.503	0.952	26.97	45.74	12.34
PtSeTe (4%)	2.139	0.443	-4.090	-6.229	0.380	0.972	30.71	47.03	14.44
PtSeTe (6%)	2.022	0.438	-4.227	-6.250	0.238	0.993	35.57	48.69	17.32
PtSeTe (8%)	1.896	0.437	-4.375	-6.271	0.089	1.014	41.42	42.87	17.76

Table S5 The band gap (E_{gap}), the difference of the electrostatic potential ($\Delta\Phi$), CBM (E_{CBM}) and VBM (E_{VBM}) refer to the vacuum level, over-potential for hydrogen evolution reaction $\chi(H_2)$, the over-Potential for oxygen evolution reaction $\chi(O_2)$, energy conversion efficiency of light absorption (η_{abs}), carrier utilization (η_{cu}) and STH (η_{STH}) efficiency in alkaline (pH = 13) environment.

Materials		E_{gap} (eV)	$\Delta\Phi$ (eV)	E_{CBM} (eV)	E_{VBM} (eV)	$\chi(H_2)$ (eV)	$\chi(O_2)$ (eV)	η_{abs} (%)	η_{cu} (%)	η_{STH} (%)
Biaxial Strain	NiSeTe (0%)	2.386	0.217	-3.829	-6.215	0.217	1.312	21.59	43.86	9.47
	NiSeTe(2%)	2.322	0.101	-3.916	-6.238	0.101	1.335	23.74	37.36	8.87
	PdSeTe (0%)	2.068	0.409	-4.024	-6.092	0.058	1.189	33.66	38.14	12.84
	PtSeTe (0%)	2.297	0.422	-3.882	-6.179	0.213	1.276	24.67	44.95	11.09
	PtSeTe(2%)	2.212	0.401	-4.006	-6.218	0.068	1.315	27.88	36.53	10.18
X Strain	NiSeTe (2%)	2.383	0.346	-3.862	-6.245	0.157	1.342	21.59	40.70	8.79
	NiSeTe (4%)	2.339	0.329	-3.931	-6.270	0.071	1.367	23.12	34.97	8.09
	PtSeTe (2%)	2.276	0.445	-3.928	-6.204	0.190	1.301	25.43	44.55	11.33
	PtSeTe (4%)	2.246	0.432	-3.975	-6.221	0.130	1.318	26.51	40.28	10.68
	PtSeTe (6%)	2.207	0.419	-4.031	-6.237	0.061	1.334	28.03	36.04	10.10
Y Strain	NiSeTe (2%)	2.335	0.346	-3.887	-6.222	0.132	1.319	23.28	39.44	9.18
	NiSeTe (4%)	2.244	0.329	-3.972	-6.216	0.030	1.313	26.66	33.85	9.03
	PtSeTe (2%)	2.235	0.450	-3.974	-6.209	0.149	1.306	26.97	41.70	11.25
	PtSeTe (4%)	2.139	0.443	-4.090	-6.229	0.026	1.326	30.71	35.03	10.76

Table S6 The calculated deformation potential (E_l), elastic modulus (C^{2D}), effective mass (m^*), mobility (μ),and relaxation time (τ) of the penta-MSeTe(M = Ni, Pd, Pt) at 300 K along x and y directions for hole and electron.

Materials	Direction	Carrier	E_l (eV)	C^{2D} (N/m)	$m^*(m_0)$	$\mu(\text{cm}^2\text{s}^{-1}\text{V}^{-1})$	$\tau(\text{fs})$
NiSeTe	x	Electron	15.26	22.78	1.83	1.24	1.29
		Hole	2.46	22.78	0.68	53.13	20.54
	y	Electron	19.34	56.95	0.46	7.68	2.00
		Hole	2.29	56.95	7.24	14.39	59.27
PdSeTe	x	Electron	3.48	28.21	1.07	51.64	31.46
		Hole	2.55	28.21	0.64	151.93	55.16
	y	Electron	3.64	54.39	0.75	130.02	55.44
		Hole	2.28	54.39	1.42	164.79	133.04
PtSeTe	x	Electron	3.36	35.70	1.62	44.86	41.32
		Hole	2.59	35.70	0.55	266.98	83.49
	y	Electron	5.06	65.70	0.53	111.28	33.53
		Hole	2.96	65.70	1.08	191.07	117.65
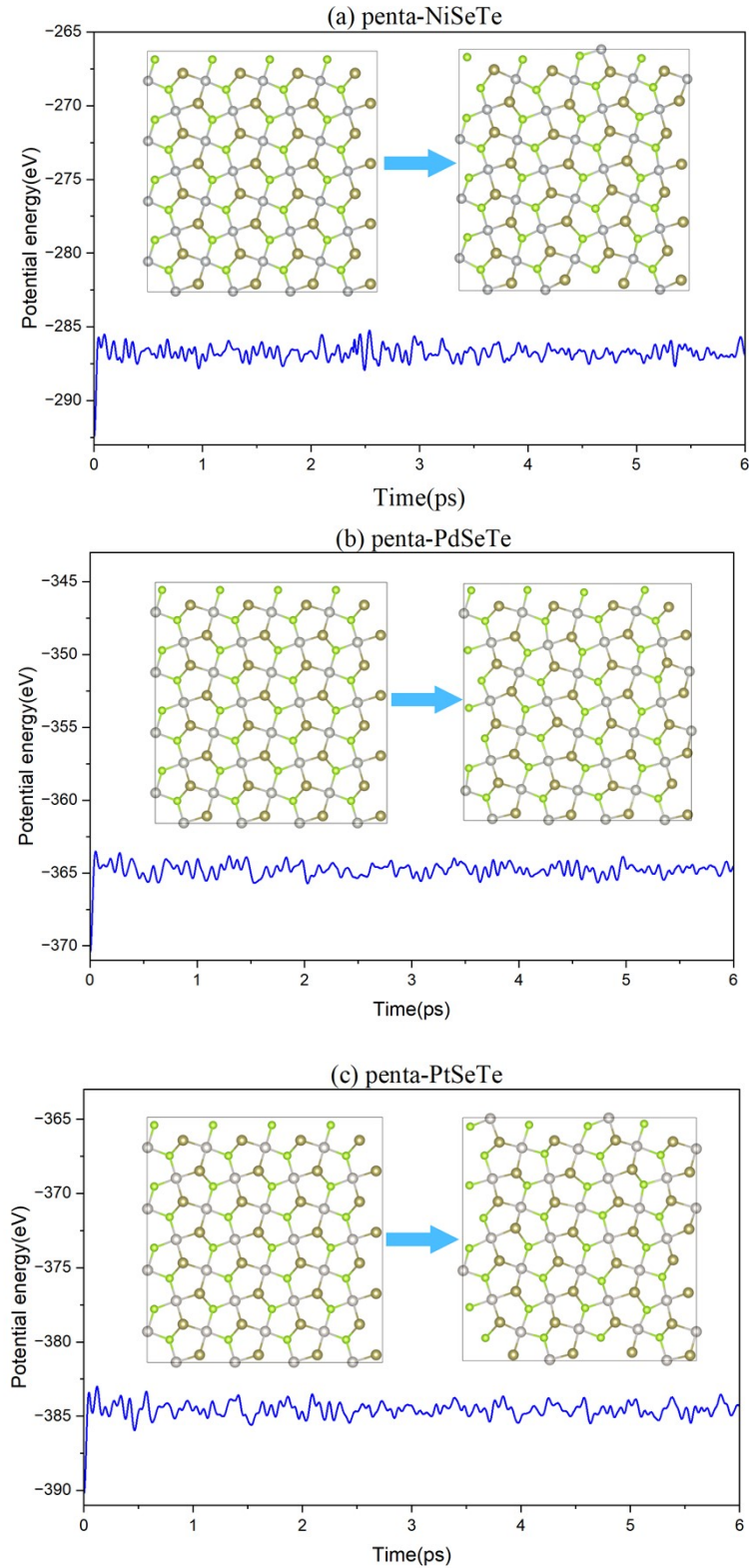
Figure S1 Potential energy fluctuations of (a) penta-NiSeTe, (b)penta-PdSeTe, (c) penta-PtSeTe

monolayers from AIMD simulations (4 × 4 × 1 supercell) at 900 K, and snapshots of initial and final

structures at 0 and 6 ps.
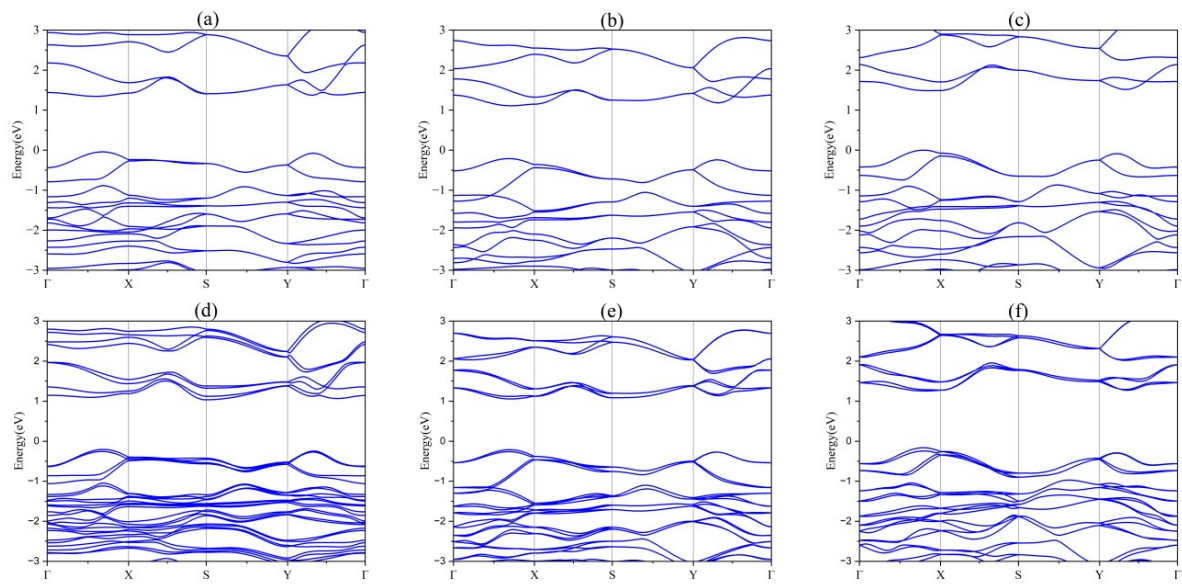
Figure S2 Band structures of (a) penta-NiSeTe, (b) penta-PdSeTe, (c) penta-PtSeTe at the PBE level and band structures of (d) penta-NiSeTe, (e) penta-PdSeTe, (f) penta-PtSeTe at the PBE+SOC level.
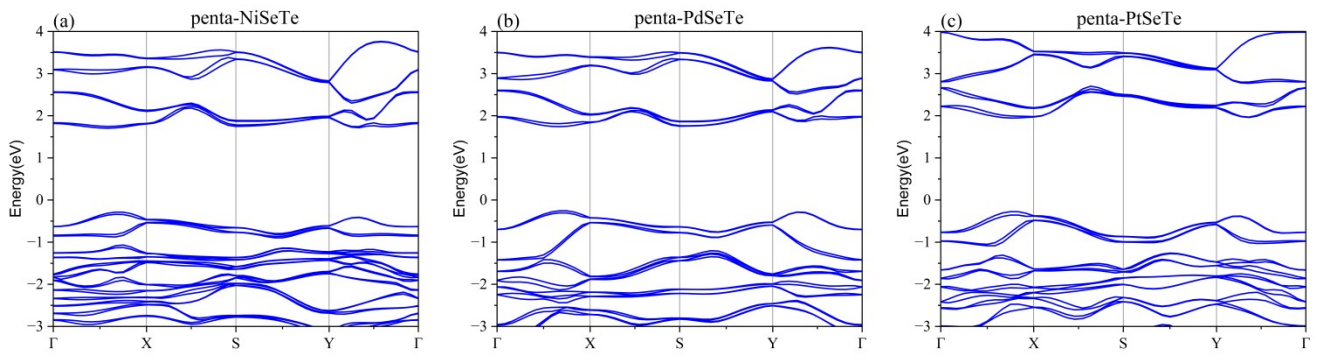
Figure S3 Band structures of (a) penta-NiSeTe, (b) penta-PdSeTe, (c) penta-PtSeTe at the HSE06+SOC level.
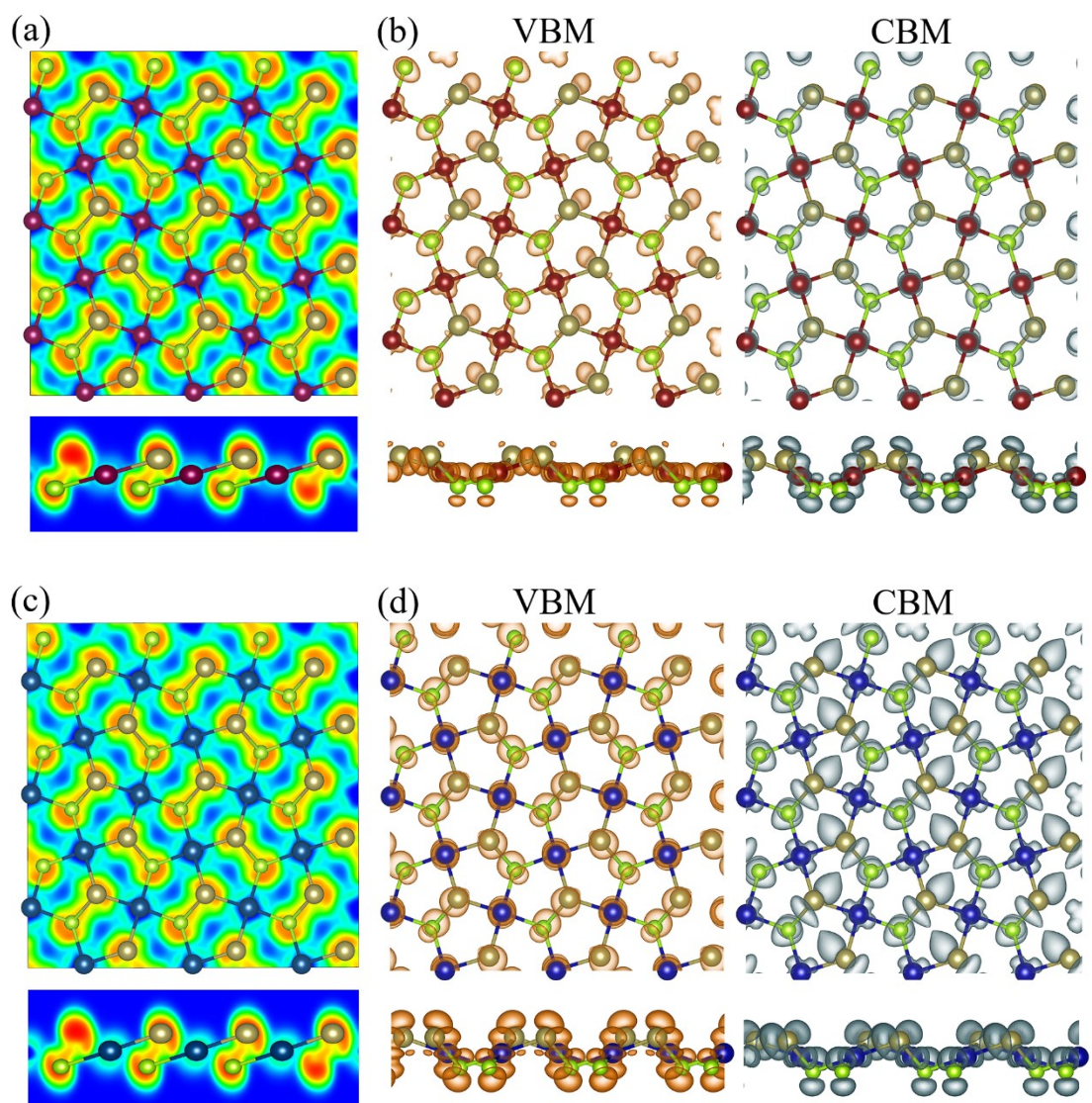
Figure S4 (a) (c) electron localization function and (b) (d) partial charge densities of the VBM (left) and CBM (right) for penta-NiSeTe and penta-PdSeTe monolayers respectively.
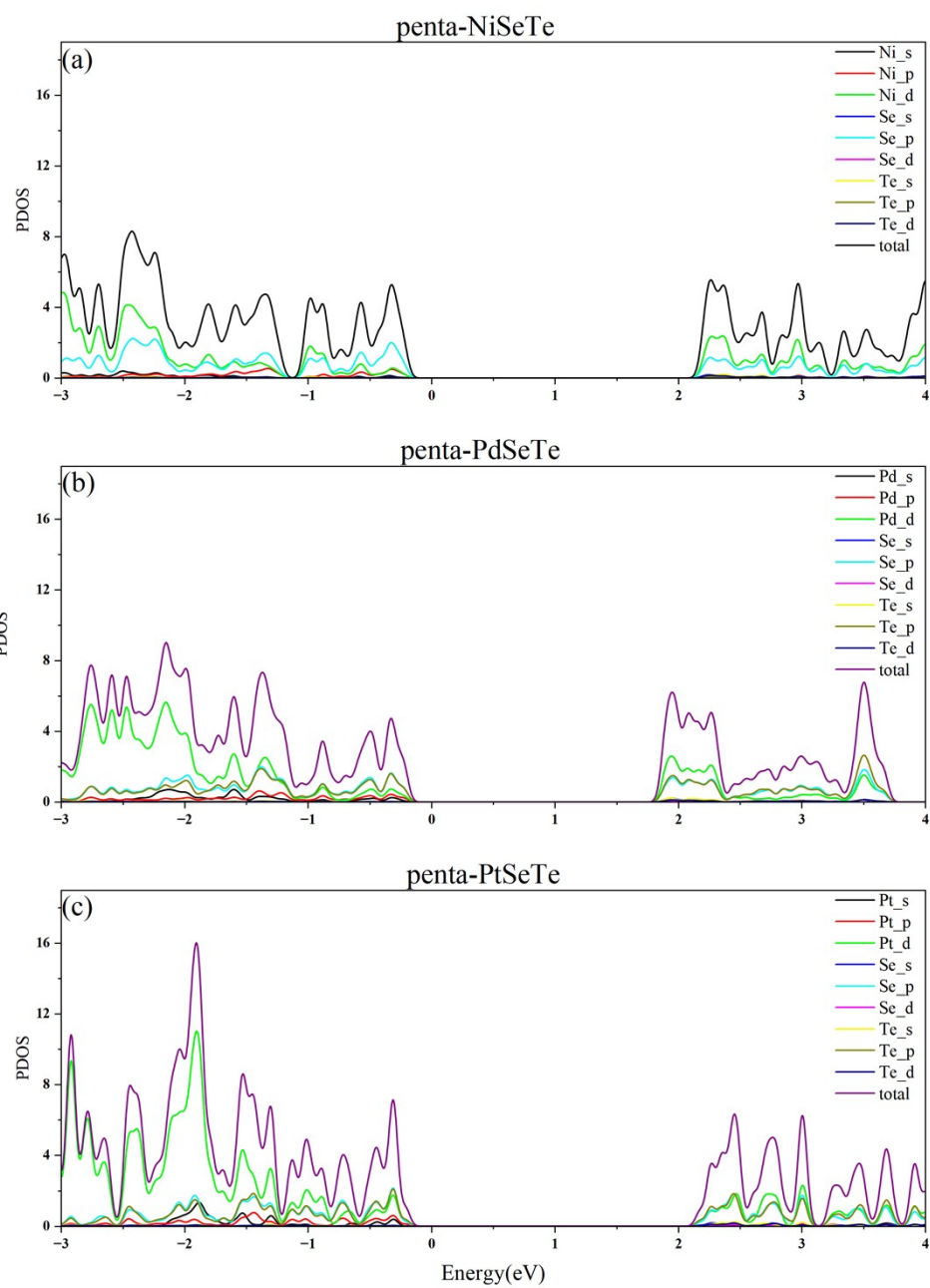
Figure S5 The calculated partial density of states (DOS) with HSE06 functional of penta-MSeTe monolayers.
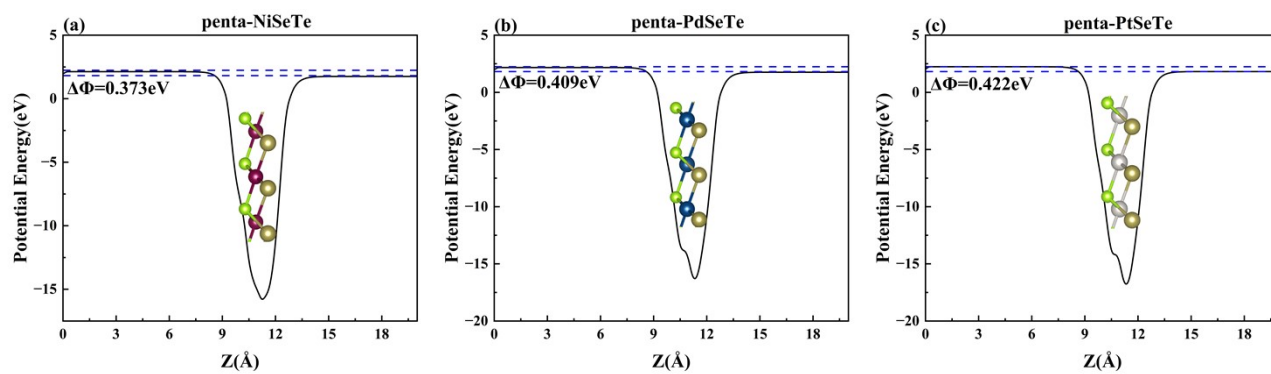
Figure S6 The plane average electrostatic potentials of penta-MSeTe monolayers: (a) penta-NiSeTe, (b) penta-PdSeTe, and (c) penta-PtSeTe.
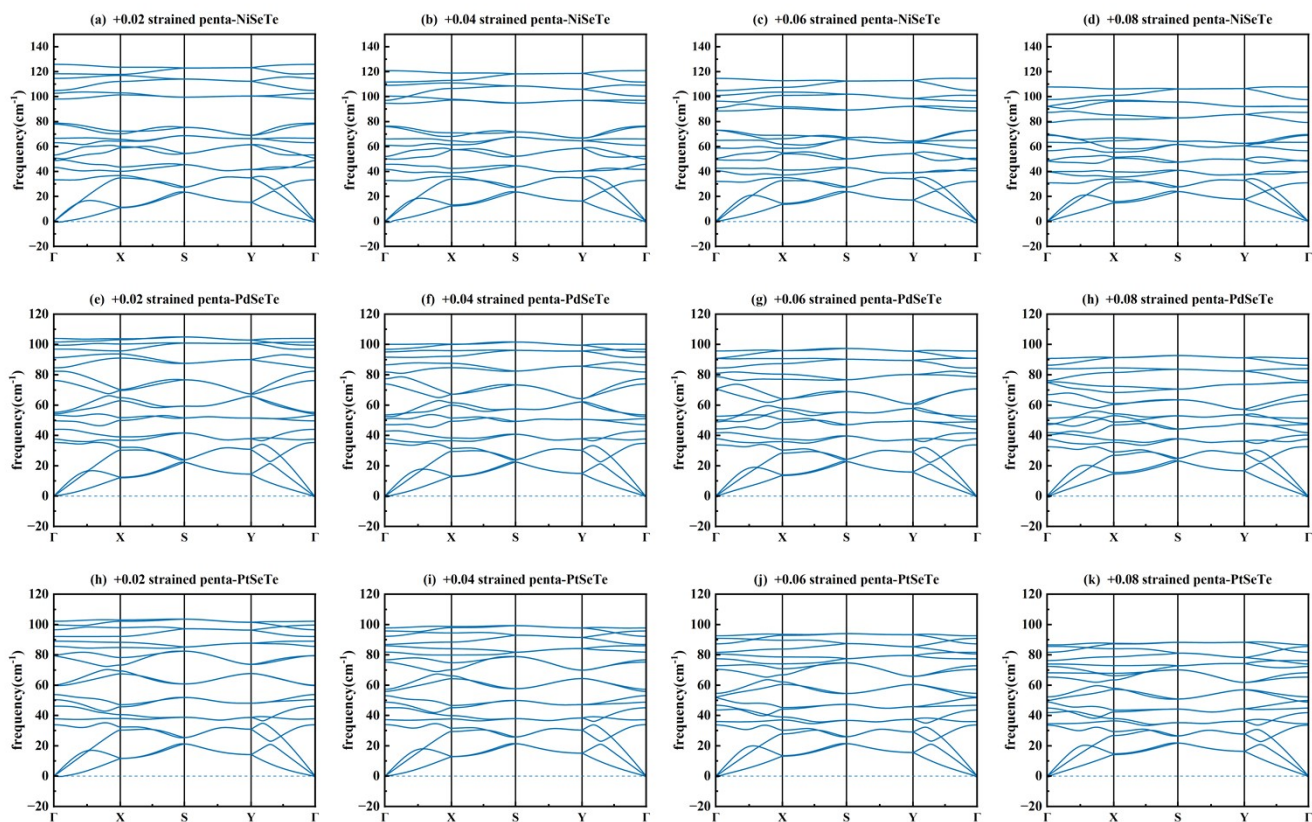
**Figure S7** The phonon disperions of penta-MSeTe under +2% to +8% biaxial strain
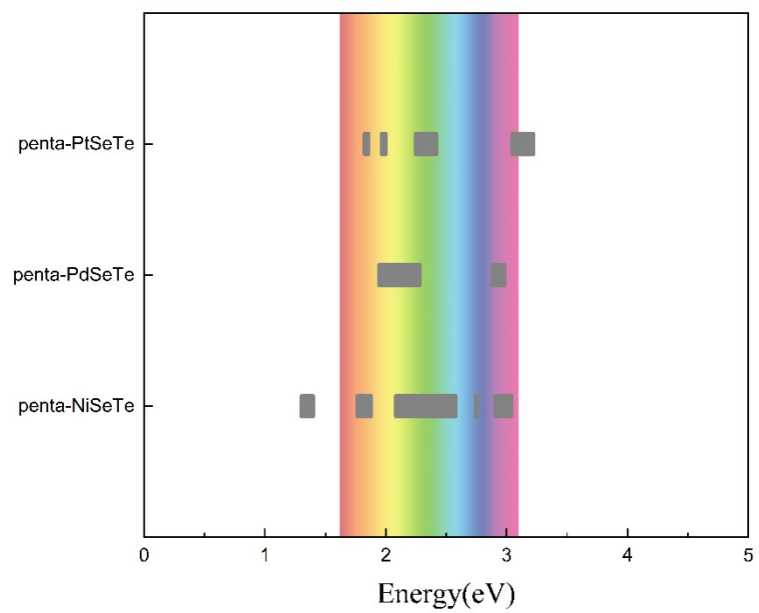
Figure S8 The hyperbolic region marked in grey of penta-MSeTe. The visual spectrum is indicated in color.